J. Iron Steel Res. Int. (2021) 28:809–817
https://doi.org/10.1007/s42243-021-00590-6

ORIGINAL PAPER

Thermal analysis and kinetic modeling of pulverized coal combustion accompanied with coke breeze

Peng Han[1] · Wen-long Zhan[1] · Hao-bin Zhu[1] · Lei Gao[2] · Ying-chang Yu[3] · Zhi-jun He[1] · Jun-hong Zhang[1] · Qing-hai Pang[1]

Received: 21 April 2020 / Revised: 16 September 2020 / Accepted: 17 September 2020 / Published online: 13 April 2021

Abstract
Pulverized coal injection technique has been widely used as a means of reducing coke consumption during ironmaking process. Owing to the increasing shortage of fossil fuels, other substitutes such as biomass, plastic, and waste tires have been studied in recent years. Coke breeze as one of the by-products of coking industries has been investigated as a substitute for partial pulverized coals. The combustion characteristics of blended fuels were estimated based on the flammability index *C* and the combustion characteristic index *S*. For different coke breeze additions, the combustion was divided into two stages, and the apparent kinetic parameters of the two stages were estimated by fitting the experimental data to the shrinkage reaction model and shrinkage diffusion model, respectively. Results showed that with the increase in coke breeze addition from 15% to 60%, the indexes *C* and *S* decrease, and the activation energy of the first stage remains almost constant, while that of the last stage increases from 16.89 up to 67.18 kJ mol^{-1}, which indicates that adding coke breeze decreases the combustion efficiency of pulverized coal. Comparing the combustion and kinetic parameters under different coke breeze addition conditions, the optimal addition amount is suggested to be within 15%.

Keywords Blast furnace · Pulverized coal injection · Coke breeze · Combustion · Kinetic model

1 Introduction

Recently, there has been an increasing emission of greenhouse gases in the world, 70% of which are attributed to the production of iron and steel [1]. For an increasing environmental concern associated with limited supply of coking coals, the blast furnace (BF) route is required to reduce its amount of CO_2 emissions. To promote sustainability in ironmaking, a number of researches have been carried out to provide a more sustainable and efficient alternative to fossil fuel-based energy and reductants such as coke and coal with renewable energy sources such as waste plastics, biomass materials and $CO-H_2$-based gas mixtures [2–5]. Wang et al. [6] reported the combustion reactivity of biomass and coal mixture, and the experimental results showed that biomass had catalytic effects on the combustion of coal. Babich et al. [7] have also reported the industrial-scale test for charcoal injection into the BF. Therefore, the use of coke breeze as one of the by-products in the coking industries has been reported as a solid fuel in sintering plants [8]. Ansteel, for example, has an excess of approximately 0.3 t of coke breeze per month, except for supplies in sintering. The replacement of anthracite coals by coke breeze in pulverized coal injection (PCI), though theoretically feasible considering similarities of the two fuels, has been successfully mixed with bituminous coals in several BFs of China in practical production, providing the need for validation of the vital significance of combustion properties of mixed fuels [9–11].

The original online version of this article was revised: table 3 was not correct.

✉ Wen-long Zhan
zhanwenlong288@163.com

✉ Lei Gao
glkust2013@hotmail.com

[1] School of Materials and Metallurgy, University of Science and Technology Liaoning, Anshan 114051, Liaoning, China

[2] Key Laboratory of Green-Chemistry Materials in University of Yunnan Province, Yunnan Minzu University, Kunming 650504, Yunnan, China

[3] Ansteel Engineering Technology Corporation Limited, Anshan 114021, Liaoning, China

Relevant researches on combustion kinetics of mixed fuels are mainly focused on employing a single reaction model to describe the whole process. Fei et al. [12] found that the random pore model (RPM) was better to fit the experimental data. Sadhukhan et al. [13] deduced a shrinking core model (SCM) to analyze the dynamics of coal char combustion and evaluated the accuracy with experimental data. Furthermore, Sun et al. [14] compared the kinetic parameters of coal char with different models including RPM, unreacted SCM and volumetric model; however, the rate-determining step of the coal combustion process is not actually a single chemical reaction, and thus more kinetic models should be taken into consideration for different reaction processes.

In this paper, non-isothermal thermogravimetry [15–19] is employed to carry out the combustion experiments among Taixi anthracite, Hongliulin bituminous coal, and coke breeze. Based on the combustion characteristic parameters, the reaction process is divided into two stages. Then, the appropriate models are presented to describe the reaction process in different temperature ranges. The kinetic parameters such as activation energy, reaction rate constants and effective diffusion coefficient can be obtained at different intervals, and the optimum addition amount of coke breeze for PCI is proposed, which may help to reduce the greenhouse gas emission in BF production.

2 Experimental

2.1 Materials

Taixi coal (TA) is one of the anthracitic coals located in Ningxia Province, China, while Hongliulin coal (HB) is one of the bituminous coals located in Shanxi Province, China. TA and HB are widely used in BFs of Ansteel. The proximate analysis and ultimate analysis of the mentioned two coals and coke breeze (CB) are shown in Table 1. According to the requirements of coal quality for PCI [20, 21], the volatile content of mixed fuels used in the experiments is limited within the range of 15–20 wt.%. The mixing ratio of HB is kept as 40% to illustrate the influence of replacing TA with CB on the combustion properties of mixed fuels as shown in Table 2.

2.2 Methodology

A comprehensive thermogravimetric analyzer Netzsch No. STA 449 F3 was used for the testing of the sample, and approximately 15 mg of the mixed fuel sample (75–150 μm) was prepared, which was then heated from room temperature to 1000 °C, at a heating rate of 20 °C min^{-1} and airflow rate of 100 mL min^{-1}. The mass loss and weightlessness rate were expressed by thermogravity (TG) and differential thermogravimetry (DTG) curves of the sample, respectively, and automatically recorded by a computer. Finally, the conversion curve and conversion rate curve of mixed fuel combustion were obtained based on related calculations. The conversion rate of reaction (α) at time t is defined as follows:

$$\alpha = \frac{m_0 - m_t}{m_0 - m_f} \quad (1)$$

where m_0 is the initial mass of the sample, mg; m_t is the mass of sample at reaction time t, mg; and m_f is the final mass of the sample at the end of the test, mg.

Table 2 Composition of each mixed fuel sample (%)

Sample No.	HB	TA	CB
S1	40	60	0
S2	40	45	15
S3	40	30	30
S4	40	15	45
S5	40	0	60

Table 1 Proximate analysis and ultimate analysis of different fuels (wt.%)

Fuel	Proximate analysis (air dried basis)				Ultimate analysis				
	M	A	V	FC	C	H	N	O	S
HB	1.82	11.21	32.44	54.53	69.48	4.24	1.56	11.12	0.56
TA	0.70	5.56	8.38	85.36	81.40	3.42	1.32	2.42	0.07
CB	0.98	6.03	1.98	91.01	92.54	0.49	1.04	0.95	0.13

M Moisture; A ash; V volatile; FC fixed carbon

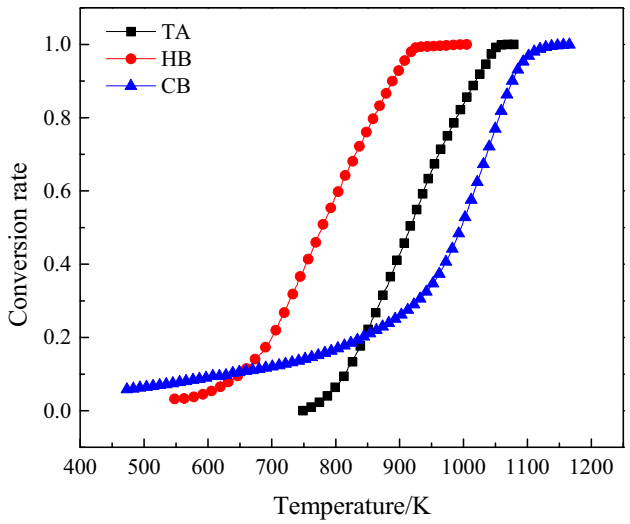

Fig. 1 Fractional conversion curves of different fuels

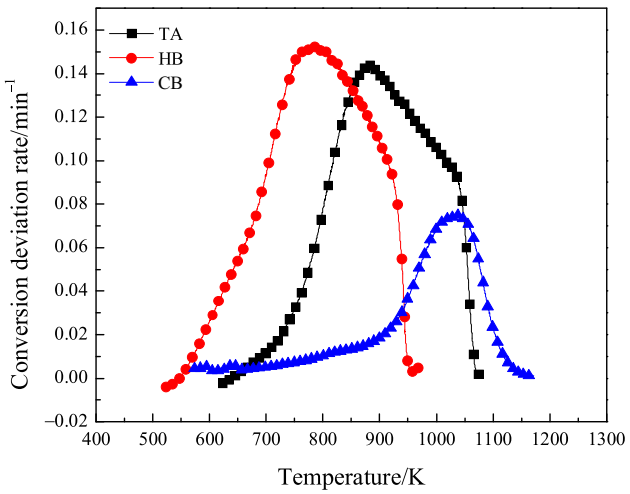

Fig. 2 Conversion deviation rate curves of different fuels

3 Results and discussion

3.1 Combustion characteristics analysis

The conversion rate and the conversion deviation rate curves of different fuels are shown in Figs. 1 and 2. The

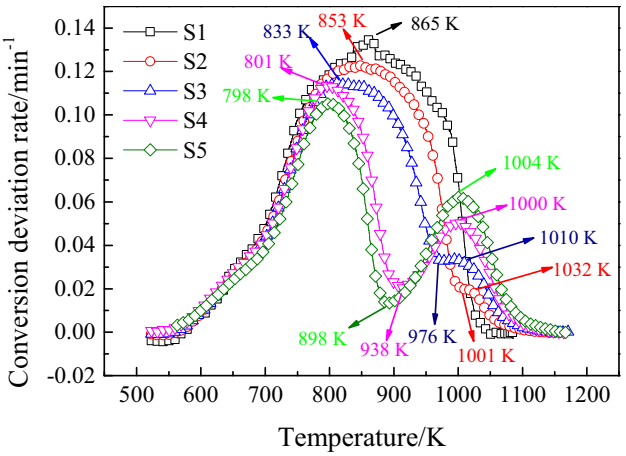

Fig. 3 Conversion deviation rate curves of mixed fuel combustion

results showed a distinct phenomenon of mass loss caused by evaporation of water at around 373 K. According to the TG–DTG principles, the ignition temperature of coal can be obtained, and the flammability index C and the combustion characteristic index S can be calculated by Eqs. (2) and (3), respectively.

$$C = \frac{W_{\max}}{T_{\mathrm{i}}^2} \tag{2}$$

$$S = \frac{W_{\max} \cdot W_{\mathrm{mean}}}{T_{\mathrm{i}}^2 T_{\mathrm{f}}} \tag{3}$$

where T_{i} is the ignition temperature, K; T_{f} is the burnout temperature, K; $W_{\max}$ is the maximum conversion rate in the combustion process, % min^{-1}; and W_{mean} is the mean conversion rate in the combustion process, % min^{-1}.

Results in Table 3 show that the T_{i} and T_{f} of CB were the highest, and thus the indexes C and S were the lowest, indicating that the CB had the worst combustion performance. Besides, the T_{i} and T_{f} of TA are higher than those of HB, which shows that the combustion performance of TA was inferior to that of HB.

Five samples of the mixed fuel were analyzed (S1, S2, S3, S4, and S5), four of which (S2, S3, S4, and S5) exhibited a double peak phenomenon as shown in Fig. 3. However, the reaction mechanism for the initial and later

Table 3 Combustion characteristic parameters of single fuel

Sample No.	T_{i}/K	T_{f}/K	$W_{\max}$/(% min^{-1})	W_{mean}/(% min^{-1})	C/(% min^{-1} K^{-2})	S/(%^{2} min^{-2} K^{-3})
TA	753	1059	14.2	9.7	2.50×10^{-5}	2.29×10^{-7}
HB	645	942	15.3	10.8	3.68×10^{-5}	4.22×10^{-7}
CB	835	1110	7.5	3.7	1.08×10^{-5}	3.61×10^{-8}

Table 4 Combustion characteristics parameters of mixed fuels

Sample No.	T_i/K	T_f/K	W_{max}/(% min^{-1})	W_{mean}/(% min^{-1})	C/(% min^{-1} K^{-2})	S/(%^{2} min^{-2} K^{-3})
S1	660	996	13.6	7.24	3.12×10^{-5}	2.27×10^{-7}
S2	646	1009	12.4	7.11	2.97×10^{-5}	2.09×10^{-7}
S3	633	1040	11.6	6.09	2.90×10^{-5}	1.70×10^{-7}
S4	631	1059	11.4	4.89	2.86×10^{-5}	1.32×10^{-7}
S5	622	1071	10.7	4.47	2.77×10^{-5}	1.15×10^{-7}

stages was different. The driving force at the initial stage is mainly chemical reaction, but it gradually changes to internal diffusion at the later stage of the combustion.

In addition, in the low-temperature zone (temperature $T < 773$ K), CB in the mixed fuel basically does not react due to a higher T_i, and it is mainly the combustion of HB and TA, while in the high temperature zone ($T > 973$ K), the combustion of the TA and CB plays a leading role. The combustion characteristic parameters of mixed fuels are listed in Table 4.

Since the combustion property of HB coal is better than that of TA, the T_i of the mixed fuels decreases gradually, and the T_f increases from 996 to 1071 K. Taking the other operational parameters into account, the addition of coke breeze in mixed fuels will worsen the combustion performance of pulverized coal. Furthermore, compared with S1, the flammability index for the other samples (S2, S3, S4, and S5) decreased by 4.8%, 7.1%, 8.3%, and 11.2%, respectively, and the combustion characteristic index decreased by 18.9%, 29.0%, 39.6% and 46.7%, respectively. However, when the CB addition is higher than 15%, the combustion performance of the mixed fuels deteriorates greatly. This result can provide a reference for PCI in actual production and thus improve the utilization of CB.

3.2 Kinetic modeling of mixed fuel combustion

The subsection method, as a kinetic analysis method based on rate-determining steps in different reaction stages, is mainly used for analyzing the pyrolysis of pulverized coal [22]. In Eq. (4), for example, the product layers were not formed at the initial stage, which is mainly controlled by chemical reaction [23–25]. However, at the end of this stage, the product layer was formed, and then the diffusion of the gaseous reactants and products became the main rate-determining step.

$$\mathrm{A(g)} + b\mathrm{B(s)} = g\mathrm{G(g)} + \mathrm{Ash} \tag{4}$$

The reaction rate can be calculated by Eq. (5):

$$v = -\frac{\mathrm{d}n_\mathrm{A}}{\mathrm{d}t} = -\frac{\mathrm{d}n_\mathrm{B}}{b\mathrm{d}t} = -\frac{4\pi r_t^2 \rho_\mathrm{B} \mathrm{d}r_t}{bM_\mathrm{B}\mathrm{d}t} \tag{5}$$

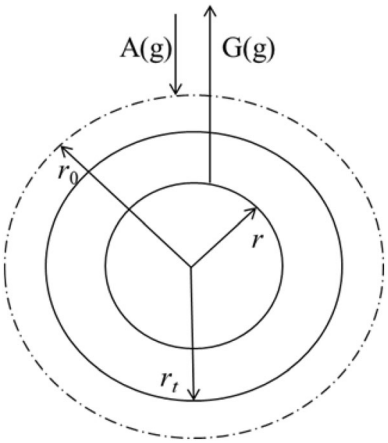

Fig. 4 Schematic diagram of chemical reaction model

where v is the reaction rate of combustion, mol s^{-1}; n_A and n_B are the molar amount of reactant A and B, respectively, mol; r_t is the radius of reactant B at time t, m; M_B is the molar mass of reactant B, kg mol^{-1}; and ρ_B is the density of reactant B, kg m^{-3}.

Considering different reaction models, we have the following models.

Model 1: interface chemical reaction model

The SCM is selected as shown in Fig. 4, assuming that pulverized coal particles were spheres, and that the speed control stage was a first-order interface chemical reaction [26].

Under the condition for the interface chemical reaction control, the reaction rate can be calculated as follows:

$$v_\mathrm{B} = -\frac{\mathrm{d}n_\mathrm{A}}{\mathrm{d}t} = 4\pi r_t^2 k_\mathrm{rea} c_\mathrm{Ab} \tag{6}$$

where v_B is the reaction rate of reactant B, mol s^{-1}; k_rea is the rate constant of interface chemical reaction, m s^{-1}; and c_Ab is the concentration of gas in the gas phase, mol m^{-3}.

Further, Eq. (7) can be obtained by combining Eqs. (5) and (6):

$$v = -\frac{4\pi r_t^2 \rho_\mathrm{B} \mathrm{d}r_t}{bM_\mathrm{B}\mathrm{d}t} = 4\pi r_t^2 k_\mathrm{rea} c_\mathrm{Ab} = v_\mathrm{B} \tag{7}$$

Then, it is simplified as follows:

$$-\frac{\rho_B}{bM_B c_{Ab}}dr_t = k_{rea}dt \tag{8}$$

Substituting $dT = \beta dt$ and $k_{rea} = A\exp[-E_1/(RT)]$ in Eq. (8), the kinetic model under non-isothermal conditions can be derived by employing Coats–Redfern integral equation.

$$\ln\frac{G_1(\alpha)}{T^2} = \ln\frac{\delta_1 AR}{\beta E_1} - \frac{E_1}{RT} \tag{9}$$

where

$$G_1(\alpha) = 1-(1-\alpha)^{1/3}; \quad \alpha = \left(r_0^3 - r_t^3\right)/r_0^3;$$
$$\delta_1 = bM_B c_{Ab}/(\rho_B r_0);$$

T is the reaction temperature at time t, K; β is the heating rate, K min^{-1}; A is the pre-exponential factor of the reaction, m s^{-1}; E_1 is the activation energy of the interface chemical reaction, J mol^{-1}; R is the molar gas constant, J mol^{-1} K^{-1}; and r_0 is the initial radius of reactant B, m.

From the linear fitting between $\ln[G_1(\alpha)/T^2]$ and $1/T$, E_1 and A were calculated. Finally, the relationship between k_{rea} and T is obtained.

Model 2: internal diffusion model with shrinking core volume

The combustion of the later stage is controlled by diffusion. Considering the actual reaction conditions, this stage is described by the internal diffusion model with the shrinking core volume. The internal diffusion rate in the product layer can be expressed as:

$$v_D = -\frac{dn_A}{dt} = 4\pi r_t^2 D_{eff}\frac{dc_A}{dr_t} \tag{10}$$

where v_D is the rate of internal diffusion, mol s^{-1}; D_{eff} is the effective diffusion coefficient of reactant A, m^2 s^{-1}; and c_A is the concentration of reactant A, mol m^{-3}.

The reaction rate for reactant B is as follows:

$$v_B = -\frac{dn_B}{bdt} = -\frac{4\pi r_t^2 \rho_B dr_t}{bM_B dt} \tag{11}$$

Using the same method, Eq. (12) is obtained by synthesizing Eqs. (10) and (11).

$$v_D = 4\pi r_t^2 D_{eff}\frac{dc_A}{dr_t} = -\frac{4\pi r_t^2 \rho_B dr_t}{bM_B dt} = v_B \tag{12}$$

Then, it is simplified as follows:

$$D_{eff}\frac{dc_A}{dr_t} = -\frac{\rho_B dr_t}{bM_B dt} \tag{13}$$

Substituting $dT = \beta dt$ and $D_{eff} = D_0\cdot\exp[-E_2/(RT)]$ in Eq. (13), the internal diffusion–reaction model can be derived by employing Coats–Redfern integral equation.

$$\ln\frac{G_2(\alpha)}{T^2} = \ln\frac{\delta_2 D_0 R}{\beta E_2} - \frac{E_2}{RT} \tag{14}$$

where

$$G_2(\alpha) = 1 - 2/3\alpha - (1-\alpha)^{2/3}; \quad \delta_2 = 2bM_B c_{Ab}/\left(\rho_B r_0^2\right);$$

D_0 is the diffusion coefficient in the standard state, m^2 s^{-1}; and E_2 is the diffusion activation energy, J mol^{-1}.

Similarly, from the linear fitting between $\ln[G_2(\alpha)/T^2]$ and $1/T$, E_2 and D_0 can be calculated according to the slope and intercept of the straight line. Finally, the relationship between D_{eff} and T is obtained.

3.3 Modeling fitting results

Based on the above analysis, the experimental data are substituted in Eqs. (9) and (14) for linear fitting. The demarcation point of the rate-determining step is judged by the linear correlation degree. In order to improve the linear correlation of the experimental data fitting, the two curves at the initial and later steps were simultaneously fitted by the two models to obtain a much more accurate demarcation point of temperature.

According to the results of the above derivation, the experimental data are substituted in Eqs. (9) and (14), respectively, for linear fitting, where $\rho_B = 1.29 \times 10^3$ kg m^{-3}, $r_0 = 1.12 \times 10^{-4}$ mm, $c_{Ab} = 8.58$ mol m^{-3}, $b = 1$, and $M_B = 2.91 \times 10^{-2}$ kg mol^{-1}.

The slope, intercept and correlation coefficient were obtained based on fitting, and then the activation energy and pre-exponential factors were obtained. Substituting the obtained activation energy and pre-exponential factor in the equation $k_{rea} = A\cdot\exp[-E_1/(RT)]$ and $D_{eff} = D_{0}\cdot\exp[-E_2/(RT)]$, the relationship of the reaction rate constant and effective diffusion coefficient to the temperature at two stages is obtained.

The kinetic parameters of initial and later stages of combustion process for different fuels are listed in Tables 5 and 6, respectively. Figures 5 and 6 illustrate that the experimental data were well fitted. The pre-reaction model was a chemical reaction model with a small activation energy, and then for the later stage, the activation energy was large and the internal diffusion of the gas product became the main rate-controlling step due to the existence of the product layer. It is observed in Fig. 3 that the mixed fuel S1 without coke breeze has only one peak, and the mixed fuels S2–S5 with different proportions of coke breeze have two peaks of different degrees, and as the proportion of coke breeze added increases, the second peak becomes larger. The main reason is that the reaction speed control links in the initial and late stages of combustion are different. In the initial stage, the chemical reaction speed is

Table 5 Kinetic parameters of combustion in initial stage

Sample No.	E_1/(kJ mol^{-1})	A/(m s^{-1})	k_{rea}/(m s^{-1})	Correlation coefficient R^2
S1	49.80	20.32	$\ln k_{rea} = -5990/T + 3.01$	0.9941
S2	39.31	4.31	$\ln k_{rea} = -4728/T + 1.46$	0.9936
S3	39.17	4.33	$\ln k_{rea} = -4711/T + 1.46$	0.9942
S4	37.26	3.72	$\ln k_{rea} = -4480/T + 1.31$	0.9898
S5	36.71	3.27	$\ln k_{rea} = -4415/T + 1.18$	0.9863

Table 6 Kinetic parameters of combustion in later stage

Sample No.	E_2/(kJ mol^{-1})	D_0/(m s^{-1})	D_{eff}/(m s^{-1})	R^2
S2	16.89	2.56×10^{-6}	$\ln D_{eff} = -2031/T - 12.88$	0.9901
S3	28.75	7.81×10^{-6}	$\ln D_{eff} = -3458/T - 11.76$	0.9949
S4	50.77	4.23×10^{-5}	$\ln D_{eff} = -6107/T - 10.07$	0.9950
S5	67.18	1.23×10^{-4}	$\ln D_{eff} = -8080/T - 9.00$	0.9956

dominant, while in the later stage, the internal diffusion speed is controlled. The mixed fuel of bituminous coal and anthracite in S1 has a fast enough chemical reaction speed in the initial stage. The violent reaction makes the fuel exhausted. In the later period, the diffusion process is short and can be ignored, and the second peak does not appear, so that in Fig. 6, the calculation of the effective diffusion coefficient for S1 is not performed.

Table 7 shows the combustion reaction rate constant and diffusion coefficient of each sample at 400–800 °C, where M is the ratio of decrease of each sample compared to S1 or S2:

$$M = \frac{k_{reai} - k_{rea1}}{k_{rea1}} \times 100\% \quad (15)$$

$$M = \frac{D_{effi} - D_{eff2}}{D_{eff2}} \times 100\% \quad (16)$$

where k_{reai} is the reaction rate constant for the combustion of mixed fuel S$_i$ (i = 2, 3, 4, 5), m s^{-1}; k_{rea1} is the reaction rate constant of mixed fuel S1, m s^{-1}; D_{effi} is the diffusion coefficient for the combustion of mixed fuel S$_i$ (i = 3, 4, 5), m s^{-1}; and D_{eff2} is the effective diffusion coefficient for the combustion of mixed fuel S2, m s^{-1}.

With the increase in CB mass fraction, the change in the trend of the k_{rea} and D_{eff} is different. The k_{rea} increases slightly in the earlier stage, which corresponds to the previous conclusions, but the D_{eff} decreases greatly in the later stage. This shows that the increase in the mass fraction of the CB has a great influence on the later diffusion process, which is not conducive to the stable and smooth operation of the BF. As the content of CB in the mixed fuel increases, both the flammability index and the combustion characteristic index decrease, and the reaction activation energy increases greatly in the later stage of combustion, indicating that a large amount of CB will reduce the combustion performance of the mixed fuel. Comparing the combustion characteristics and kinetic parameters of mixed fuels with different coke breeze contents, it is acceptable to use a small amount of coke breeze replacing pulverized coal for high injection under the condition of ensuring the smooth operation of the blast furnace. Combined with the results in Sect. 3.1, it is believed that the mass fraction of the CB for the pulverized coal injected into the BF should be controlled within 15%, which ensures the stable combustion of the pulverized coal and can make good use of the coke breeze. Considering the price of coke breeze, calorific value, and other factors, different steel plants should determine the amount of addition according to their actual conditions.

4 Conclusions

1. With the increase in the amount of CB, the ignition point and burnout point of pulverized coal increase correspondingly, and the flammability index and the combustion characteristic index both decrease, indicating that the addition of CB reduces the combustion performance of pulverized coal.
2. The dynamic analysis of the combustion process of coal/coke breeze mixed fuel is carried out by the subsection method. Shrinking core models of interface chemical reaction and internal diffusion were used to model the process at the earlier stage and the later stage to obtain the kinetic parameters, respectively. The results showed that with increasing CB content in blended fuels, the activation energy at the earlier stage

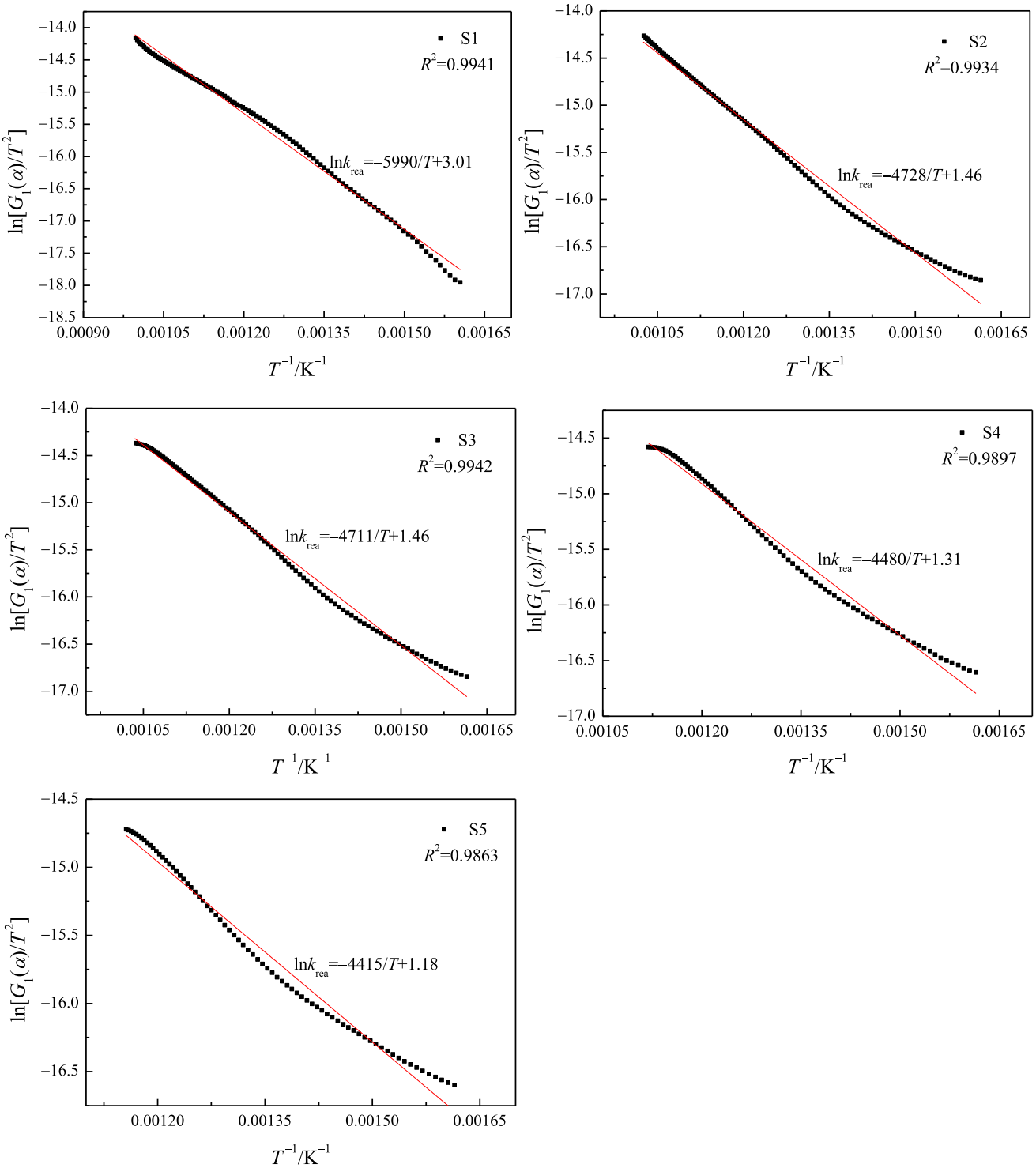

Fig. 5 Linear fitting of rate-determining step controlled by chemical reaction in initial stage

decreased slightly, but the activation energy at the later stage increased significantly, and the trends of k_{rea} and D_{eff} were consistent with the trend of the activation energy, which further shows that the addition of CB reduces the combustion performance of pulverized coal.

3. Comparing the combustion characteristics and kinetic parameters of the mixed fuel with different CB contents, the mass fraction of the CB should be controlled within 15%.

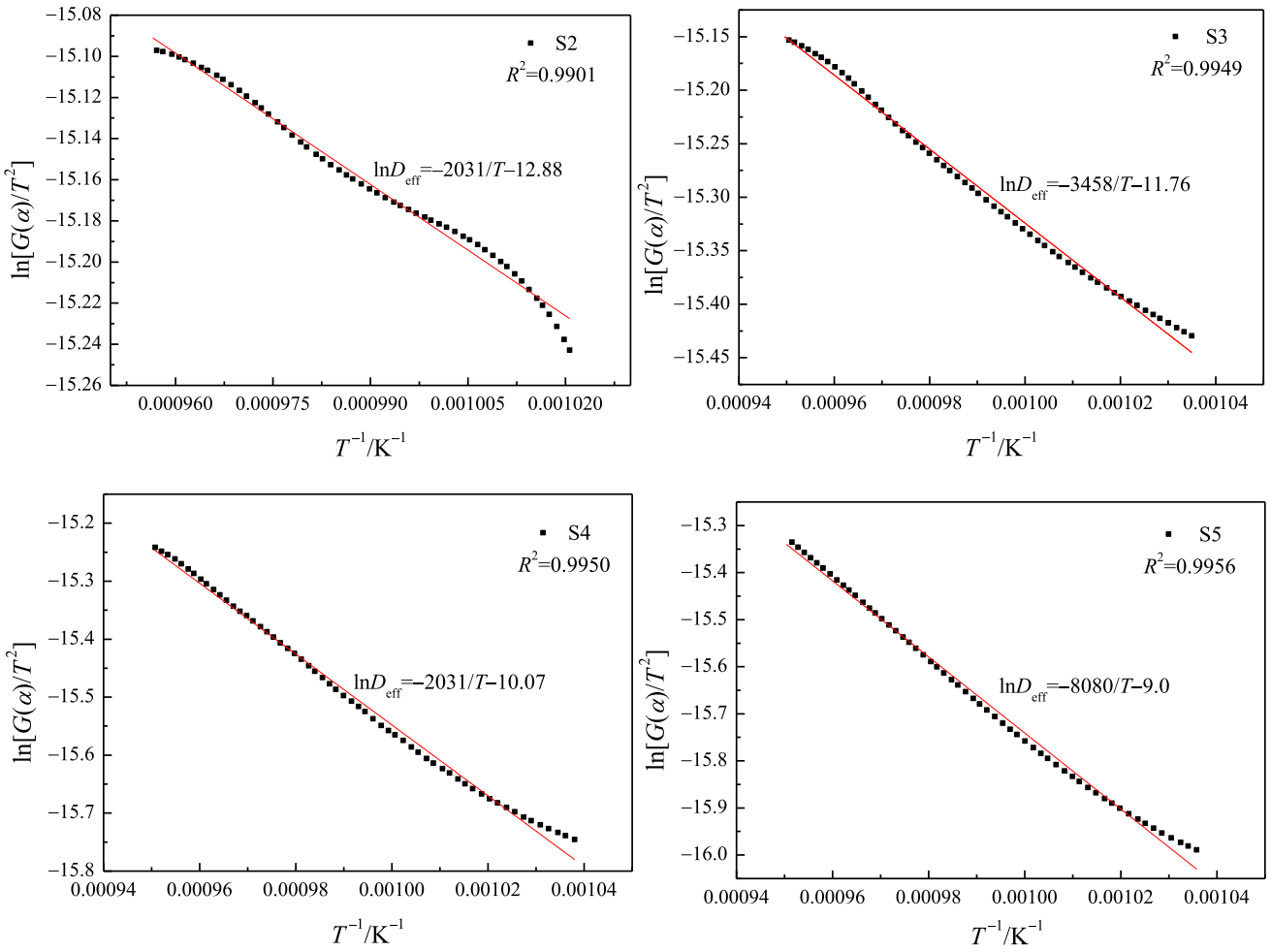

Fig. 6 Linear fitting of speed control period by diffusion in later stage

Table 7 Reaction rate constant and diffusion coefficient of blended fuels

Reaction temperature/°C	Parameter	S1	S2	S3	S4	S5
400	k_{rea}/(m s^{-1})	2.77×10^{-3}	3.85×10^{-3}	3.93×10^{-3}	4.75×10^{-3}	4.61×10^{-3}
	M	–	38.99	41.88	71.48	66.43
500	k_{rea}/(m s^{-1})	8.74×10^{-3}	9.47×10^{-3}	9.75×10^{-3}	1.13×10^{-2}	1.08×10^{-2}
	M	–	8.35	11.56	29.29	23.57
600	k_{rea}/(m s^{-1})	2.13×10^{-2}	1.93×10^{-2}	1.95×10^{-2}	2.19×10^{-2}	2.07×10^{-2}
	M	–	− 4.41	− 8.45	2.82	− 2.82
700	D_{eff}/(m s^{-1})	–	1.2×10^{-6}	2.24×10^{-7}	8.59×10^{-8}	3.06×10^{-8}
	M	–	–	− 81.33	− 92.84	− 97.45
800	D_{eff}/(m s^{-1})	–	3.85×10^{-7}	3.12×10^{-7}	1.43×10^{-7}	6.62×10^{-8}
	M	–	–	− 18.96	− 62.86	− 82.81

Acknowledgements Thanks are given to the financial supports from the National Natural Science Foundation of China (Nos. 51604148, 51874171, and 51974154).

References

[1] G.W. Wang, J.L. Zhang, W.W. Chang, R.P. Li, Y.J. Li, C. Wang, Energy 147 (2018) 25–35.
[2] X.J. Ning, H.P. Teng, G.W. Wang, J.L. Zhang, N. Zhang, C.C. Huang, C. Wang, Fuel 270 (2020) 117526.
[3] D. Wang, S.Y. Luo, Y.M. Zhou, C.J. Yi, J. Iron Steel Res. Int. 25 (2018) 330–339.
[4] Q. Wang, J.L. Zhang, G.W. Wang, H.Y. Wang, M.M. Sun, Energy Fuels 32 (2018) 2145–2155.
[5] D.B. Huang, Y.B. Zong, R.F. Wei, W. Gao, X.M. Liu, J. Iron Steel Res. Int. 23 (2016) 874–883.
[6] J. Wang, S.Y. Zhang, X. Guo, A.X. Dong. C. Chen, S.W. Fang, Y.T. Fang, W.D. Yin, Energy Fuels 26 (2012) 7120–7126.
[7] A. Babich, D. Senk, J. Solar, I. de Marco, ISIJ Int. 59 (2019) 2212–2219.
[8] L.M. Lu, M. Adam, M. Kilburn, S. Hapugoda, M. Somerville, S. Jahanshahi, J.G. Mathieson, ISIJ Int. 53 (2013) 1607–1616.
[9] T. Xu, G.W. Wang, J.L. Zhang, T.F. Song, R.S. Xu, J. Iron Steel Res. Int. 24 (2017) 985–990.
[10] C. Zou, J.X. Zhao, X.M. Li, R.M. Shi, J. Therm. Anal. Calorim. 126 (2016) 1469–1480.
[11] Y.J. Li, J.L. Zhang, G.W. Wang, W. Liang, N. Zhang, P.M. Guo, Ironmak. Steelmak. 47 (2020) 228–237.
[12] H. Fei, P.S. Li, Q.J. Gu, Y. Liu, Energy Fuels 31 (2017) 14280–14287.
[13] A.K. Sadhukhan, P. Gupta, R.J. Saha, Int. J. Chem. Kinet. 40 (2008) 569–582.
[14] H. Sun, J.L. Zhang, G.W. Wang, J.G. Shao, X.H. Peng, Chin. J. Process Eng. 14 (2014) 114–119.
[15] T. Xu, X.J. Ning, G.W. Wang, W. Liang, J.L. Zhang, Y.J. Li, H.Y. Wang, C.H. Jiang, Int. J. Miner. Metall. Mater. 25 (2018) 1412–1422.
[16] H.Y. Jiang, J.G. Wang, S.Q. Wu, B.S. Wang, Z.Z. Wang, Carbon 48 (2010) 352–358.
[17] R.L. Du, K. Wu, L. Zhang, Y. She, D.A. Xu, C.Y. Chao, X.K. Qian, B. Zhang, J. Therm. Anal. Calorim. 125 (2016) 959–966.
[18] R. Zan, W. Wang, R.S. Xu, J. Schenk, H. Zheng, H.X. Wang, Energies 12 (2019) 4324.
[19] D.K. Seo, S.S. Park, J. Hwang, T.U. Yu, J. Anal. Appl. Pyrolysis 89 (2010) 66–73.
[20] S. Vyazovkin, K. Chrissafis, M.L.D. Lorenzo, N. Koga, M. Pijolat, B. Roduit, N. Sbirrazzuoli, J.J. Sunol, Thermochim. Acta 590 (2014) 1–23.
[21] C. Zou, J.Y. He, J.X. Zhao, X.M. Li, R.M. Shi, C. Ma, Y. Kang, X.R. Zhang, Metall. Mater. Trans. B. 50 (2019) 2304–2318.
[22] L.M. Zhou, T.A. Luo, Q.W. Huang, Energy Convers. Manage. 50 (2009) 705–710.
[23] W.S. Seames, Fuel Process. Technol. 81 (2003) 109–125.
[24] C.Y. Tsai, A.W. Scaroni, Fuel 66 (1987) 1400–1406.
[25] N.C. Beck, A.N. Hayhurst, Combust. Flame 79 (1990) 47–74.
[26] W. Qian, Q. Xie, Y.Y. Huang, J.T. Dang, K.D. Sun, Q. Yang, J.C. Wang, Int. J. Min. Sci. Technol. 22 (2012) 645–650.